

RESEARCH ARTICLE

10.1002/2014PA002751

Key Points:

- AMOC recovery leads to ~ 0.5 permil $\delta^{18}\text{O}_c$ decrease in the deep North Atlantic
- Benthic $\delta^{18}\text{O}_c$ changes are mainly driven by temperature changes
- Meltwater input, climate change, and temperature effect equally affect surface $\delta^{18}\text{O}_c$

Supporting Information:

- Readme
- Figure S1
- Figure S2
- Figure S3
- Figure S4
- Figure S5
- Figure S6
- Figure S7
- Figure S8
- Table S1

Correspondence to:

W. Bagniewski,
w.bagniewski@student.unsw.edu.au

Citation:

Bagniewski, W., K. J. Meissner, L. Menviel, and C. E. Brennan (2015), Quantification of factors impacting seawater and calcite $\delta^{18}\text{O}$ during Heinrich Stadials 1 and 4, *Paleoceanography*, 30, 895–911, doi:10.1002/2014PA002751.

Received 13 NOV 2014

Accepted 19 JUN 2015

Accepted article online 25 JUN 2015

Published online 20 JUL 2015

Quantification of factors impacting seawater and calcite $\delta^{18}\text{O}$ during Heinrich Stadials 1 and 4Witold Bagniewski¹, Katrin J. Meissner¹, Laurie Menviel¹, and Catherine E. Brennan²

¹Climate Change Research Centre and ARC Centre of Excellence for Climate System Science, University of New South Wales, Sydney, New South Wales, Australia, ²Department of Oceanography, Dalhousie University, Halifax, Nova Scotia, Canada

Abstract We perform idealized experiments of a Heinrich Stadial using an oxygen-isotope-enabled Earth System Climate Model. Our results compare relatively well with the planktic and benthic $\delta^{18}\text{O}$ records of Heinrich Stadials 1 and 4. We find that changes in surface $\delta^{18}\text{O}_c$ can be equally attributed to the “temperature effect” due to fractionation during calcification; the “circulation and climate effect” due to changes in circulation, precipitation, and evaporation; and the “meltwater effect” due to the addition and subsequent advection of depleted fresh water from continental ice sheets. In contrast, the meltwater effect and circulation and climate effect have only a small impact on benthic $\delta^{18}\text{O}_c$ during the cessation of the Atlantic Meridional Overturning Circulation (AMOC). Significant temperature changes simulated in both the deep Atlantic and Pacific Oceans substantially influence benthic $\delta^{18}\text{O}_c$ during that time. During the AMOC recovery, however, anomalously low $\delta^{18}\text{O}_w$ surface waters are advected to the deep Atlantic, thus generating a large (~ 0.5 ‰) $\delta^{18}\text{O}_c$ decrease in the deep North Atlantic. This is in contrast to a hypothesis that links such depletion seen in Atlantic sediment cores during the last glacial stadials to deepwater formation caused by brine rejection and sea ice formation.

1. Introduction

The last glacial period was punctuated by millennial-scale events during which the formation of North Atlantic Deep Water (NADW) weakened significantly [e.g., *Sarnthein et al.*, 2001; *Kissel et al.*, 2008; *Menviel et al.*, 2014a]. These events, called Heinrich events [*Heinrich*, 1988], occurred at the end of longer-term cooling periods and were associated with massive iceberg discharges into the North Atlantic. Heinrich events had a global impact on climate [e.g., *Wang et al.*, 2001; *Huber et al.*, 2006; *Fleitmann et al.*, 2009; *Deplazes et al.*, 2013] and the carbon cycle [e.g., *Ahn and Brook*, 2014].

Oxygen isotope records from ice cores, corals, and marine sediments can help us to reconstruct these events and give us a better understanding of the climate feedbacks at play. For example, the oxygen isotope composition of calcium carbonate shells ($\delta^{18}\text{O}_c$) collected from ocean sediment cores may serve as a proxy record of seawater temperature [*Urey*, 1948]. However, $\delta^{18}\text{O}_c$ does not only depend on temperature but also on the isotopic composition of the water in which the shells form [*Shackleton*, 1967]. Heinrich iceberg armadas originated predominantly from the Laurentide ice sheet [e.g., *MacAyeal*, 1993; *Alley et al.*, 2006] and to a lesser extent from other ice sheets surrounding the North Atlantic Ocean [*Peck et al.*, 2007]. These icebergs added meltwater, which was depleted in ^{18}O , to the North Atlantic. This addition of isotopically light meltwater must have had a significant effect on the $\delta^{18}\text{O}$ values of seawater ($\delta^{18}\text{O}_w$) and thus foraminiferal $\delta^{18}\text{O}_c$. Within a given sediment core, the variations in foraminiferal $\delta^{18}\text{O}_c$ can therefore be decomposed into three contributions: the change related to global ice volume variations (and therefore sea level variations); the change related to local seawater $\delta^{18}\text{O}_w$ variations; and the change related to local ocean temperature variations. Distinguishing between these factors is a major challenge in paleoceanography [*Waelbroeck et al.*, 2011], a challenge that can be tackled with numerical simulations performed with oxygen-isotope-enabled models.

Fully coupled three-dimensional isotope-enabled climate models are a very recent addition to the large and diverse family of climate models. To the authors' knowledge, this study is the fifth of its kind simulating $\delta^{18}\text{O}$ during a glacial stadial with a fully coupled isotope-enabled climate model [*Lewis et al.*, 2010; *Brennan et al.*, 2012, 2013; *Roche et al.*, 2014]. *Lewis et al.* [2010] used the coupled oxygen-isotope-enabled GISS model to study the impact of weakened NADW on the oxygen isotopic composition of precipitation. More recently, *Roche et al.* [2014] used the oxygen-isotope-enabled iLOVECLIM model to study the Atlantic basin

$\delta^{18}\text{O}$ response to different meltwater sources during Heinrich events. Changes in the oxygen isotopic composition of Pacific Ocean waters in response to weaker NADW formation rates have not been simulated yet with coupled oxygen-isotope-enabled models; neither has been the impact of NADW recovery on $\delta^{18}\text{O}$.

In this study, we simulate an idealized Heinrich Stadial with the isotope-enabled University of Victoria Earth System Climate Model (UVic ESCM) [Brennan *et al.*, 2012, 2013] to analyze the respective impacts of the three main contribution factors to $\delta^{18}\text{O}_c$ recorded in foraminifera: the addition of ^{18}O -depleted meltwater in the North Atlantic and its propagation (the “meltwater signal”); anomalies in seawater $\delta^{18}\text{O}_w$ due to changes in ocean circulation, evaporation, precipitation, river discharge, sea ice formation, and melt (“circulation and climate signal”); and changes in water temperature (“temperature effect signal”). Simulated seawater $\delta^{18}\text{O}_w$ and carbonate $\delta^{18}\text{O}_c$ are compared with 36 sediment cores from both the Atlantic and Pacific basins and covering Heinrich Stadials 1 and 4.

Furthermore, we analyze one puzzling aspect of paleoproxy records from the Nordic Seas during Heinrich events: depletions in benthic $\delta^{18}\text{O}_c$ of approximately -1‰ at a time when NADW formation was thought to be weak or completely shut off [e.g., Rasmussen *et al.*, 1996; Rasmussen and Thomsen, 2004; Dokken and Jansen, 1999; Kreveld *et al.*, 2000; Hillaire-Marcel and de Vernal, 2008; Meland *et al.*, 2008]. It has been suggested that rejection of isotopically light sea ice brine was responsible for transporting depleted surface $\delta^{18}\text{O}$ into deeper waters [e.g., by Veum *et al.*, 1992; Vidal *et al.*, 1998; Dokken and Jansen, 1999; Waelbroeck *et al.*, 2006; Meland *et al.*, 2008]. Newly formed sea ice is enriched in ^{18}O relative to seawater, and the expelled sea ice brine is depleted because of fractionation during sea ice formation [O’Neil, 1968]. These dense brines sink, bringing the ^{18}O -depleted, high-salinity water into the deep ocean [Hillaire-Marcel and de Vernal, 2008]. This “sea ice brine hypothesis” is supported by proxy data implying that the Nordic seas were likely ice-free in the summer [e.g., Weinelt *et al.*, 1996, 2003; Millo *et al.*, 2006] during the Last Glacial Maximum, allowing seasonal ice formation to occur. Dokken and Jansen [1999] proposed that during certain periods of the last glacial period the deep water formation shifted to a mode driven by brine formation. However, Bauch and Bauch [2001] argued that the benthic $\delta^{18}\text{O}_c$ anomalies in northern polar regions were unlikely to be driven by sea ice brine formation and suggested that the anomalies were more likely to have been caused by an intrusion of ^{18}O -depleted glacial meltwater and/or an increase in deep water temperature. Rasmussen and Thomsen [2009] also suggested that low benthic $\delta^{18}\text{O}_c$ values in the Nordic seas could not be attributed to brines, as brines with sufficient density to penetrate the deep Arctic and Nordic seas are formed from cold and salty waters and thus have high $\delta^{18}\text{O}_w$. In a recent study, Brennan *et al.* [2013] found negligible ($<0.13\text{‰}$) shifts in deep ocean $\delta^{18}\text{O}$ from interglacial-glacial sea ice variability simulated by the UVic ESCM, insufficient to explain the $\sim 1\text{‰}$ shifts found in paleoproxy. Here we follow up on the study by Brennan *et al.* [2013] and show that deep ocean $\delta^{18}\text{O}_c$ anomalies might have been caused by a large-scale recovery of the Atlantic Meridional Overturning Circulation (AMOC) at the end of a Heinrich event.

2. Methods

2.1. Model Description

The UVic ESCM, version 2.9, is a fully coupled, intermediate complexity ocean, atmosphere, land surface, vegetation, sea ice, sediment model, described by Weaver *et al.* [2001], Meissner *et al.* [2003], Schmittner *et al.* [2008], and Eby *et al.* [2009].

The ocean component of the model is the Modular Ocean Model, Version 2 [Pacanowski, 1995], an ocean general circulation model with 19 vertical levels varying from 50 m at the surface to 500 m at 5 km depth. It is coupled to a vertically integrated, two-dimensional atmospheric energy and moisture balance model, forced by seasonally varying solar insolation at the top of the atmosphere, and present-day reanalysis winds from the National Centers for Environmental Prediction (NCEP) [Kalnay *et al.*, 1996]. Atmospheric heat and moisture transport is achieved through diffusion and advection by the vertically weighted average of the NCEP monthly mean winds with superimposed geostrophic wind anomalies calculated as a function of surface temperature gradient anomalies as described in Weaver *et al.* [2001]. Moisture diffusion coefficients are described in Brennan *et al.* [2012]; they vary with latitude and are held constant in time. Other model components include a dynamic-thermodynamic sea ice model [Semtner, 1976; Hibler, 1979; Hunke and Dukowicz, 1997], a sediment model [Archer, 1996; Meissner *et al.*, 2012], and a dynamic global vegetation model MOSES/TRIFFID [Meissner *et al.*, 2003]. The UVic ESCM also includes two stable water isotopes, H_2^{18}O and H_2^{16}O , which are integrated into the ocean, atmosphere, land surface, and sea ice components of the model

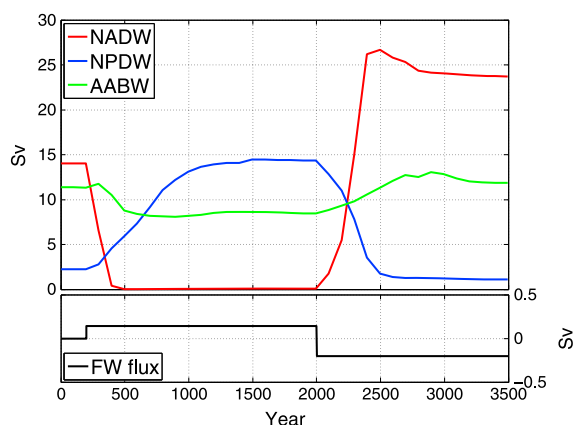


Figure 2. (top) Time series of North Atlantic Deep Water formation (NADW, red), North Pacific Deep Water formation (NPDW, blue), and Antarctic Bottom Water formation (AABW, green) rates (Sv). (bottom) A time series of the freshwater flux, where negative values represent an artificial addition of salt to force an AMOC recovery.

simulations using different meltwater isotopic ratios (-20‰ , -30‰ , and -40‰). As the simulation forced with meltwater with an isotopic signature of -20‰ (fw20) agrees best with paleoproxy data, we only show the results of that experiment in the following sections. The results of the other two experiments are shown in the supporting information.

To estimate the impact of the meltwater flux on circulation and climate change only, we perform an additional experiment (fwN) in which the freshwater hosing is not accompanied by fluxes of water isotope tracers. Hence, ocean $\delta^{18}\text{O}$ anomalies in the fwN simulation are solely due to changes in overturning circulation and resulting changes in climate patterns. By comparing fw20 to fwN, we can estimate the impact of the addition and subsequent advection of $\delta^{18}\text{O}$ -depleted meltwater.

Our model results show that North Pacific Deep Water (NPDW) formation is initiated by a shutdown of the AMOC (Figure 2), similar to previous studies [Saenko *et al.*, 2004; Okazaki *et al.*, 2010; Menviel *et al.*, 2011; Huiskamp and Meissner, 2012]. However, it is still unclear whether such a process occurred during Heinrich events. Therefore, in order to test a scenario without deep water formation in the North Pacific, additional simulations were performed, during which an additional freshwater flux without any isotopic signature was added to the North Pacific at a constant rate of 0.15 Sv for 1800 years, thus stabilizing the water column in the North Pacific (see supporting information). As the differences between the two scenarios are mostly limited to the North Pacific Ocean and do not affect the main conclusions of this study, only the results from the original two simulations will be discussed here.

Model results are compared to paleoclimate records for Heinrich Stadial 4 (HS4) and Heinrich Stadial 1 (HS1) from 36 marine sediment cores (Tables 1 and 2 and Figure 1). We focus our analysis on HS1 and HS4 because HS2 and HS3 are often difficult to identify accurately in proxy records [e.g., Menviel *et al.*, 2014a; Lynch-Stieglitz *et al.*, 2014]. For each core we determine the surface and benthic $\delta^{18}\text{O}$ Heinrich Stadial anomalies, defined as the difference between the 500 year $\delta^{18}\text{O}$ average before the beginning of a Heinrich Stadial and the 500 year average before the end of a Heinrich Stadial. Since records of the last 35 ka B.P. are generally well dated, we define HS1 $\delta^{18}\text{O}$ anomalies as the difference in 500 year averages between 15.5 ka B.P. and 17.5 ka B.P. for each core. As seen in Table 1, the time periods used to define $\delta^{18}\text{O}$ anomalies associated with HS4 correspond for most cores to 38.8 ka B.P. compared to 40.2 ka B.P.

The model simulates $\delta^{18}\text{O}$ of seawater ($\delta^{18}\text{O}_w$), which measures the departure of the sample isotopic composition from the Standard Mean Ocean Water (‰) [Baertschi, 1976]. On the other hand, the paleoproxy records represent $\delta^{18}\text{O}$ of carbonate ($\delta^{18}\text{O}_c$), which measures the departure of the sample isotopic composition from the Pee Dee Belemnite (‰) standard [Craig, 1957]. As the fractionation factor of carbonate precipitation from seawater is temperature dependent, $\delta^{18}\text{O}_c$ also includes a temperature effect. To directly compare the model results with the paleoproxy records, we add a temperature effect to the simulated $\delta^{18}\text{O}_w$. For surface (planktic) $\delta^{18}\text{O}$ we use the equation derived by Shackleton [1974]:

$$T = 16.9 - 4.38(\delta^{18}\text{O}_c - \delta^{18}\text{O}_w) + 0.10(\delta^{18}\text{O}_c - \delta^{18}\text{O}_w)^2$$

while for benthic $\delta^{18}\text{O}$ we use the equation derived by Marchitto *et al.* [2014]:

$$T = \left(0.245 - \sqrt{0.045461 + 0.0044(\delta^{18}\text{O}_c - \delta^{18}\text{O}_w)} \right) / 0.0022$$

where T is the water temperature ($^{\circ}\text{C}$).

Table 1. Heinrich Stadial Anomalies in $\delta^{18}\text{O}$ Records^a

Core	Latitude	Longitude	Depth	HS4 (ka B.P.)	$\Delta\delta^{18}\text{O}$ (‰)		$\Delta\delta^{18}\text{O}$ (‰)	HS4 Bottom	$\Delta\delta^{18}\text{O}$ (‰)	HS1 Bottom	$\Delta\delta^{18}\text{O}$ (‰)	HS1 Surface	$\Delta\delta^{18}\text{O}$ (‰)	HS4 Surface	$\Delta\delta^{18}\text{O}$ (‰)	Planktic Species	Benthic Species	Reference
					HS1 Surface	HS4 Surface												
MD95-2010	66.68	4.57	1226 m	40.2–39.3	-1.25	-0.8	-1.75	-1	-1.75	-	-0.3	-1.25	-0.8	-	-	<i>N. pach.</i> (s)	<i>C. teretis</i>	Dokken and Jansen [1999]
ENAM93-21	62.73	-4	1020 m	40.2–38.8	-1	-0.5	-1.2	-	-1.2	-	-	-1	-0.5	-	-	<i>N. pach.</i> (s)	<i>M. barle.</i>	Rasmussen et al. [1996]
SO82-5	59.19	-30.91	1416 m	40.7–39	-	0	-	0.3	-	-	-	-	0	-	-	<i>N. pach.</i> (s)	<i>C. wuell.</i>	Krevelde et al. [2000]
NA87-22	55.49	-14.69	2161 m	-	-	-	-0.6	-	-	-	-	-	-	-	-	-	<i>C. wuell.</i>	Vidal et al. [1997]
JPC13	53.06	-33.52	3082 m	40.2–38.8	-0.3	-0.8	-0.6	-0.5	-0.6	-	-	-0.3	-0.8	-	-	<i>G. bull.</i> , <i>N. pach.</i> (s)	<i>C. wuell.</i>	Hodell et al. [2010]
CH69-K09	41.75	-47.35	4100 m	-	-	-	-0.3	-	-0.3	-	-	-	-	-	-	-	<i>C. wuell.</i>	Waelbroeck et al. [2011]
MD95-2040	40.58	-9.86	2465 m	40.2–38.8	-0.65	0.2	-1	-0.8	-1	-	-	-0.65	0.2	-	-	<i>G. bull.</i>	various	Voelker and de Abreu [2011]
MD95-2042	37.8	-10.17	3146 m	40–38.8	-0.6	-0.6	-0.4	-0.4	-0.4	-	-	-0.6	-0.6	-	-	<i>G. bull.</i>	various	Shackleton et al. [2000]
MD99-2334	37.8	-10.17	3166 m	-	-0.6	-	-0.6	-	-0.6	-	-	-0.6	-	-	-	<i>G. bull.</i>	<i>G. affinis</i>	Skinner et al. [2003]
MD95-2037	37.09	-32.03	2159 m	-	-	-	-0.85	-	-0.85	-	-	-	-	-	-	-	<i>C. wuell.</i>	Labeyrie et al. [2005]
MD99-2339	35.89	-7.53	1177 m	40–38.9	-0.8	0.8	-0.85	0.3	-0.85	-	-	-0.8	0.8	-	-	<i>G. bull.</i>	various	Voelker et al. [2006]
GGC5	33.7	-57.58	4550 m	-	-1	-	-	-	-	-	-	-1	-	-	-	<i>G. infi.</i>	-	Carlson et al. [2008]
GGC51	32.78	-76.28	1790 m	-	-0.3	-	-	-	-	-	-	-0.3	-	-	-	<i>G. ruber</i> (w)	-	Carlson et al. [2008]
MD02-2575	29	-87.12	847 m	40.2–38.8	-0.2	-	-0.3	-0.1	-0.3	-	-	-0.2	-	-	-	<i>G. ruber</i> (w)	<i>U. pereg.</i>	Ziegler et al. [2008]
JPC26	24.33	-83.25	546 m	-	-0.9	-	0	-	0	-	-	-0.9	-	-	-	<i>G. ruber</i> (w)	<i>C. pachy.</i>	Lynch-Stieglitz et al. [2011]
VM28-122	11.57	-78.42	3623 m	40–38.6	-0.18	-0.2	-	-	-	-	-	-0.18	-0.2	-	-	<i>G. ruber</i> (w)	-	Schmidt et al. [2004]
m35003-4	12.09	-61.24	1299 m	-	-	-	-0.9	-	-0.9	-	-	-	-	-	-	-	<i>C. wuell.</i>	Rühlemann et al. [2004]
GeoB4905-4	2.5	9.39	1328 m	-	-0.4	-	-	-	-	-	-	-0.4	-	-	-	<i>G. ruber</i> (p)	-	Weideab et al. [2005]
MD03-2707	2.5	9.40	1295 m	40.2–38.7	-0.4	-0.3	-	-	-	-	-	-0.4	-0.3	-	-	<i>G. ruber</i> (p)	-	Weideab et al. [2007]
GeoB3129	-4.61	-36.64	830 m	-	-0.7	-	-	-	-	-	-	-0.7	-	-	-	<i>G. ruber</i> (w)	-	Weideab et al. [2006]
GeoB1711	-23.53	12.63	1967 m	40.2–38.8	-	-	-0.7	0.1	-0.7	-	-	-	-	-	-	-	<i>C. wuell.</i>	Little et al. [1997]
GGC36	-27.52	-46.47	1268 m	-	-0.38	-	-	-	-	-	-	-0.38	-	-	-	<i>G. ruber</i> (w)	-	Carlson et al. [2008]
ODP1089	-40.93	9.9	4621 m	40.2–38.8	-0.4	-	-0.5	0	-0.5	-	-	-0.4	-	-	-	<i>G. bull.</i>	<i>C. wuell.</i>	Hodell et al. [2003]
RC11-83	-41.6	9.8	4718 m	40–38.5	-0.6	-0.6	-0.35	0.15	-0.35	-	-	-0.6	-0.6	-	-	<i>N. pach.</i> (s), <i>G. bull.</i>	<i>C. mund.</i>	Charles et al. [1996]
MD07-3076Q	-44.15	-14.23	3770 m	-	-	-	-0.2	-	-0.2	-	-	-	-	-	-	-	<i>C. kullen.</i>	Waelbroeck et al. [2011]
JPC51	54.55	168.67	1466 m	-	-0.1	-	-0.45	-	-0.45	-	-	-0.1	-	-	-	<i>N. pach.</i> (s)	<i>U. pereg.</i>	Caissie et al. [2010]

Table 1. (continued)

Core	Latitude	Longitude	Depth	HS4 (ka B.P.)	$\Delta\delta^{18}\text{O}$ (‰) HS1 Surface	$\Delta\delta^{18}\text{O}$ (‰) HS4 Surface	$\Delta\delta^{18}\text{O}$ (‰) HS1 Bottom	$\Delta\delta^{18}\text{O}$ (‰) HS4 Bottom	Planktic Species	Benthic Species	Reference
MD01-2421	36.02	141.78	2224 m	40.2–38.8	-0.3	0	-0.3	0	<i>G. bull.</i> , <i>G. infl.</i>	various	<i>Oba et al.</i> [2006]
ODP893A	34.29	120.04	576 m	40.2–38.8	-1	0.5	-0.3	0.3	<i>G. bull.</i> , <i>N. pach.</i> (s)	various	<i>Hendy et al.</i> [2002]
MD97-2141	8.78	121.28	3633 m	40.2–38.8	-0.25	-	-	-	<i>G. ruber</i> (w)	-	<i>Rosenthal et al.</i> [2003]
MD98-2181	6.3	125.82	2114 m	40.2–38.8	-	0.4	-	-0.4	<i>G. ruber</i> (w)	<i>U. hisp.</i>	<i>Saikkku et al.</i> [2009]
MD97-2120	-45.53	174.93	1210 m	40–38.8	-0.2	-0.6	-	-	<i>G. ruber</i> (w)	-	<i>Pahnke et al.</i> [2003]
EW0408-85/C	59.56	-144.15	682 m	-	-0.5	-	-0.3	-	<i>N. pach.</i> (s), <i>G. bull</i>	<i>U. pereg.</i>	<i>Davies et al.</i> [2011]
EW0408-26/C	56.96	-136.43	1623 m	-	-0.45	-	-	-	<i>N. pach.</i> (s), <i>G. bull</i>	-	<i>Praetorius and Mix</i> [2014]
MD02-2503	34.28	-120.04	570 m	-	-1	-	-0.2	-	<i>G. bull.</i>	<i>U. pereg.</i>	<i>Hill et al.</i> [2006]
MD02-2529	8.20	-84.12	1619 m	40.4–39.2	-0.2	0.8	-	-	<i>G. ruber</i> (w)	-	<i>Leduc et al.</i> [2007]
TR163-22	0.51	-92.4	2830 m	40.2–38.8	-0.2	0	0	-0.25	<i>G. ruber</i> (w)	<i>U. sentic.</i>	<i>Lea et al.</i> [2006]

^a For HS1, $\Delta\delta^{18}\text{O}$ is defined as the difference in 500 year averages between 15.5 and 17.5 ka B.P. The HS4 anomalies are defined by 500 year averages between 38.8 and 40.2 ka B.P., unless otherwise stated in the table. The abbreviations for planktic and benthic species are as follows: *N. pach.* = *Neogloboquadrina pachyderma*; *G. bull.* = *Globigerina bulloides*; *G. ruber* = *Globigerinoides ruber*; *G. infl.* = *Globorotalia inflata*; *C. teretis* = *Cassidulina teretis*; *M. barle.* = *Melonis barleanum*; *C. wuell.* = *Cibicides wuellerstorfi*; *G. affinis* = *Globobulimina affinis*; *U. pereg.* = *Uvigerina peregrina*; *C. pachy.* = *Cibicides pachyderma*; *C. mund.* = *Cibicides mundulus*; *C. kullen.* = *Cibicides kullenbergi*; *U. hisp.* = *Uvigerina hispida*; *U. sentic.* = *Uvigerina senticosa*.

Table 2. Heinrich Stadial Anomalies in SST Records^a

Core	Latitude	Longitude	Depth	HS4 (ka B.P.)	Δ SST (°C)		Method	Reference
					HS1	HS4		
SO82-5	59.19	-30.91	1416 m	40.7–39	-	-1	census counts	Krevelde et al. [2000]
MD01-2443	37.9	-10.18	2925 m	40–38.8	-0.6	-3	alkenones	Martrat et al. [2007]
MD99-2339	35.89	-7.53	1177 m	40–38.9	-6	-5	census counts	Voelker et al. [2006]
GGC5	33.7	-57.58	4550 m	-	2	-	Mg/Ca	Carlson et al. [2008]
GGC51	32.78	-76.28	1790 m	-	0.5	-	Mg/Ca	Carlson et al. [2008]
MD02-2575	29	-87.12	847 m	40.2–38.8	1	-	Mg/Ca	Ziegler et al. [2008]
JPC26	24.33	-83.25	546 m	-	0	-	Mg/Ca	Schmidt and Lynch-Stieglitz [2011]
VM28-122	11.57	-78.42	3623 m	40–38.6	1	-0.4	Mg/Ca	Schmidt et al. [2004]
GeoB4905-4	2.5	9.39	1328 m	-	0.8	-	Mg/Ca	Weldeab et al. [2005]
MD03-2707	2.5	9.40	1295 m	40.2–38.7	0.8	-0.2	Mg/Ca	Weldeab et al. [2007]
GeoB3129	-4.61	-36.64	830 m	-	0	-	Mg/Ca	Weldeab et al. [2006]
GGC36	-27.52	-46.47	1268 m	-	-0.8	-	Mg/Ca	Carlson et al. [2008]
MD97-2141	8.78	121.28	3633 m	-	1	0	Mg/Ca	Rosenthal et al. [2003]
MD98-2181	6.3	125.82	2114 m	40.2–38.8	-	-0.2	Mg/Ca	Saikku et al. [2009]
MD97-2120	-45.53	174.93	1210 m	40–38.8	0	2.5	Mg/Ca	Pahnke et al. [2003]
MD02-2529	8.20	-84.12	1619 m	40.4–39.2	0.5	1	alkenones	Leduc et al. [2007]
TR163-22	0.51	-92.4	2830 m	40.2–38.8	1	0	Mg/Ca	Lea et al. [2006]

^aFor HS1, Δ SST is defined as the difference in 500 year averages between 15.5 and 17.5 ka B.P. The HS4 anomalies are defined by 500 year averages between 38.8 and 40.2 ka B.P., unless otherwise stated in the table. The SST estimates are based on foraminiferal census counts, alkenone records (U_{37}^k), and foraminiferal Mg/Ca ratios.

3. Results

3.1. Changes in Circulation

Both paleoproxy records [McManus et al., 2004; Gherardi et al., 2009; Thornalley et al., 2011; Lynch-Stieglitz et al., 2014] and modeling studies [Liu et al., 2009; Meissner et al., 2002; Menviel et al., 2011, 2014a] suggest that North Atlantic Deep Water (NADW) formation was substantially weakened during Heinrich Stadials. In our simulations, deep water formation rates are represented by the maximum of the stream function of zonally integrated meridional transport. The release of fresh water in the North Atlantic causes a shutdown of NADW formation within 200 years and a decrease in Antarctic Bottom Water (AABW) formation (Figure 2). North Pacific Deep Water (NPDW) formation strengthens over 1300 years. An artificial addition of salt to the North Atlantic leads to an overshoot recovery of NADW and AABW formation and a shutdown of NPDW formation within ~500 years.

3.2. Comparison of Simulated Changes in $\delta^{18}O$ and SST With Paleoproxy Records in the Atlantic Ocean

In order to directly compare our modeling results with paleoproxy records, we perform two types of transformations. First, we estimate model $\delta^{18}O_c$ from simulated $\delta^{18}O_w$ by adding the temperature effect using simulated surface and bottom temperatures and the equations of Shackleton [1974] and Marchitto et al. [2014], respectively. The estimated $\delta^{18}O_c$ from the simulated $\delta^{18}O_w$ and SST is thus associated with the uncertainty of the regression slopes ($\delta^{18}O_c/SST$). In the second transformation, we employ independent paleoproxy SST information (Table 2) to remove the temperature effect from paleoproxy-derived $\delta^{18}O_c$, thus determining paleoproxy $\delta^{18}O_w$. The uncertainty for this second transformation is therefore larger, adding the temperature proxy uncertainty (based on Mg/Ca, alkenones, or census counts) to the uncertainty of the $\delta^{18}O_c/SST$ slope. We present surface isotope and temperature anomalies (Δ), defined as the difference between 10 year averages for year 2000 and year 0 (control), in Figure 3. We compare the simulated $\Delta\delta^{18}O_w$ to the proxy-estimated $\Delta\delta^{18}O_w$ (Figure 3a) and alternatively the simulated $\Delta\delta^{18}O_c$ to the proxy $\Delta\delta^{18}O_c$ (Figure 3b). Zonal average results for the deep Atlantic and Pacific Oceans are presented in Figures 4 and 5, respectively.

As seen in Figure 3a, an AMOC shutdown caused by the addition of -20% $\delta^{18}O_w$ meltwater to the North Atlantic leads to a $\delta^{18}O_w$ decrease of 1 to 2.5‰ at the surface of the North Atlantic and a 0.25 to 1.25‰

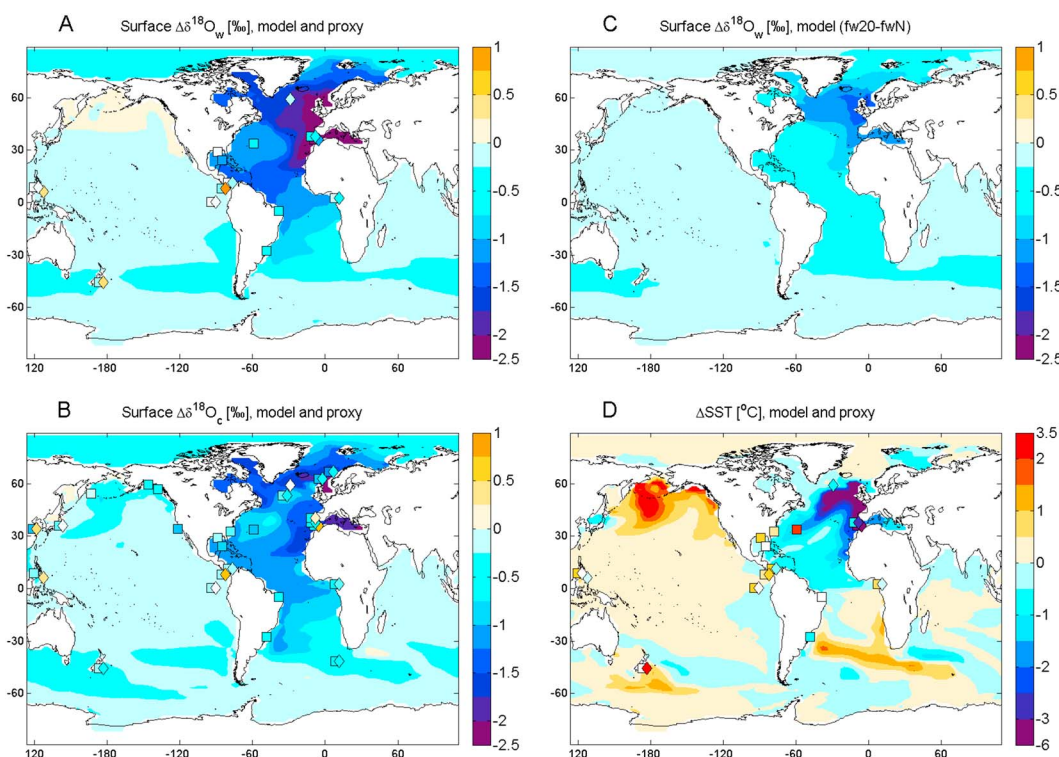


Figure 3. Surface anomalies (Δ , year 2000 minus year 0) simulated in experiment fw20, superimposed by paleoproxy anomalies for HS1 (squares) and HS4 (diamonds): (a) model $\delta^{18}O_w$ and proxy $\delta^{18}O_w$; (b) model $\delta^{18}O_c$ and proxy $\delta^{18}O_c$; (c) meltwater signal (see section 3.3); and (d) model and proxy SST. It should be noted that we are only showing the results for the model's first level (0–50 m) because most of the planktic records presented here are of surface-dwelling foraminifera (Table 1).

decrease at the surface of the South Atlantic. The accompanying reduction in meridional ocean heat transport leads to a simulated North Atlantic SST decrease of up to 5.6°C in agreement with paleoproxy results (Figure 3d). At the surface of the North Atlantic, the weaker meridional transport of low-latitude high $\delta^{18}O_w$ waters to high latitudes leads to negative $\delta^{18}O_w$ anomalies (Figure 6c). Lower surface temperatures reduce evaporation, which leads to an additional decrease in $\delta^{18}O_w$. The impact of North Atlantic cooling on $\delta^{18}O_c$ tends to offset the $\delta^{18}O_w$ decrease due to meltwater input. But, in agreement with most proxy records for both HS1 and HS4, $\delta^{18}O_c$ decreases at the surface of the Atlantic with the greatest decrease observed in the North Atlantic (Figure 3b). We overestimate the $\delta^{18}O_c$ decrease at the surface of the north East Atlantic by ~0.8‰. Since –20‰ is at the higher range of the isotopic signature of meltwater input and since the experiment fwN underestimates the north East Atlantic $\delta^{18}O_c$ decrease (see supporting information), this would indicate that we are adding too much fresh water in our simulations, i.e., that the sea level increase associated with HS1 and HS4 was more likely on the order of 10 m, in agreement with *Chappell* [2002].

The model simulates a decrease in $\delta^{18}O_w$ over the entire Atlantic basin, ranging from 0.1‰ below 3000 m depth to more than 1‰ above 600 m depth (Figure 4a). When the temperature effect is included, cooling in the North Atlantic caused by a partial replacement of NADW by colder AABW results in an increase in the simulated $\delta^{18}O_c$ by up to 0.5‰ between 500 and 4000 m depth (Figure 4b). This is not supported by benthic paleoproxy records for HS1 (squares in Figure 4b), which consistently show a decrease in $\delta^{18}O_c$ at all depths. However, the simulated $\delta^{18}O_c$ is in relatively good agreement with three HS4 records (diamonds) between 1000 and 2000 m depth where $\delta^{18}O_c$ does indeed increase. The model-data agreement is also relatively good at depths greater than 3500 m, where both simulated and recorded $\delta^{18}O_c$ decrease by up to 0.5‰ (Figure 4b).

The fact that the recorded change in $\Delta\delta^{18}O_c$ during HS1 and HS4 is of opposite sign between 500 and 2500 m depth suggests that subsurface Atlantic circulation might have been different during the two stadials. To test the $\Delta\delta^{18}O_c$ records against different modes of circulation, we show $\delta^{18}O_c$ anomalies calculated based

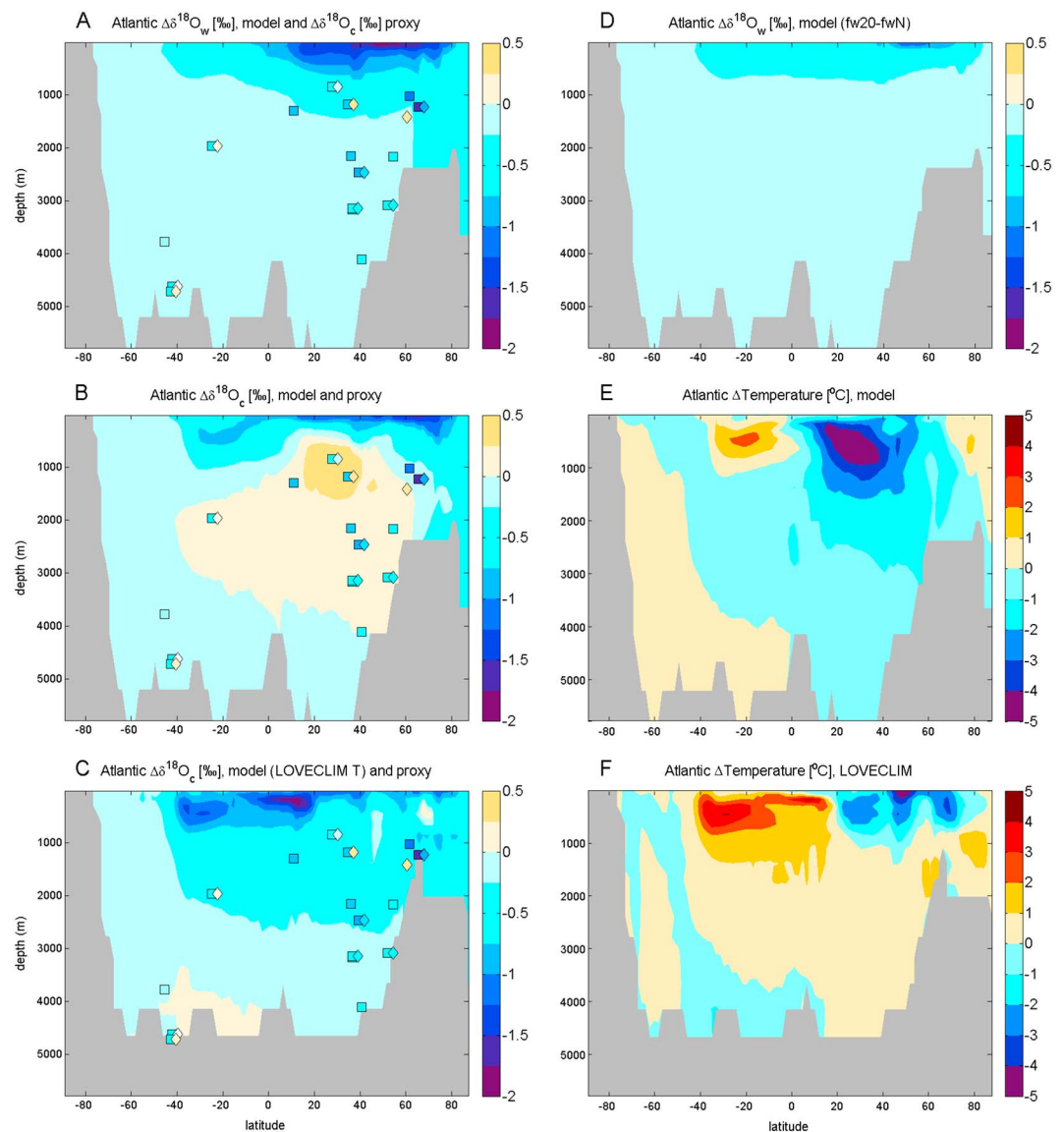


Figure 4. Anomalies (Δ , year 2000 minus year 0) simulated in experiment fw20 in the Atlantic Ocean (zonal average), superimposed by paleoproxy $\delta^{18}\text{O}_c$ anomalies for HS1 (squares) and HS4 (diamonds): (a) $\delta^{18}\text{O}_w$; (b) $\delta^{18}\text{O}_c$; and (c) $\delta^{18}\text{O}_c$ calculated using temperature anomalies from a meltwater experiment performed with LOVECLIM [Menviel et al., 2014b]. (d) Difference between fw20 and fwN $\delta^{18}\text{O}_w$ anomalies, representing the meltwater signal. Temperature anomalies averaged over the Atlantic basin for (e) experiment fw20 performed with the UVic ESCM and (f) a meltwater experiment performed with LOVECLIM [Menviel et al., 2014b].

on a model simulation without a significant intrusion of AABW in Figure 4c. Figure 4c was generated using simulated water temperatures obtained in a similar meltwater experiment and performed with the LOVECLIM model [Menviel et al., 2014b]. Since the version of the LOVECLIM model we use does not include oxygen isotopes, we combine the simulated temperature anomalies (Figure 4f) with the UVic ESCM $\delta^{18}\text{O}_w$ anomalies (Figure 4a) to calculate $\Delta\delta^{18}\text{O}_c$ shown in Figure 4c. Due to the reduced meridional oceanic heat transport to the North Atlantic, the North Atlantic cools while the South Atlantic warms in both models. However, the South Atlantic warming is greater in LOVECLIM, possibly due to weaker southeasterly trades in that model. The South Atlantic warming penetrates to depth and is maximum at about 500 m depth. Due to the continued suppression of convection of cold surface water to the deep North Atlantic, the deep North Atlantic slowly warms by diffusion, in general agreement with a previous study [Brady and Otto-Bliesner, 2011]. The simulated North Atlantic warming in LOVECLIM leads to a $\delta^{18}\text{O}_c$ decrease, which agrees within 0.5‰ with most benthic

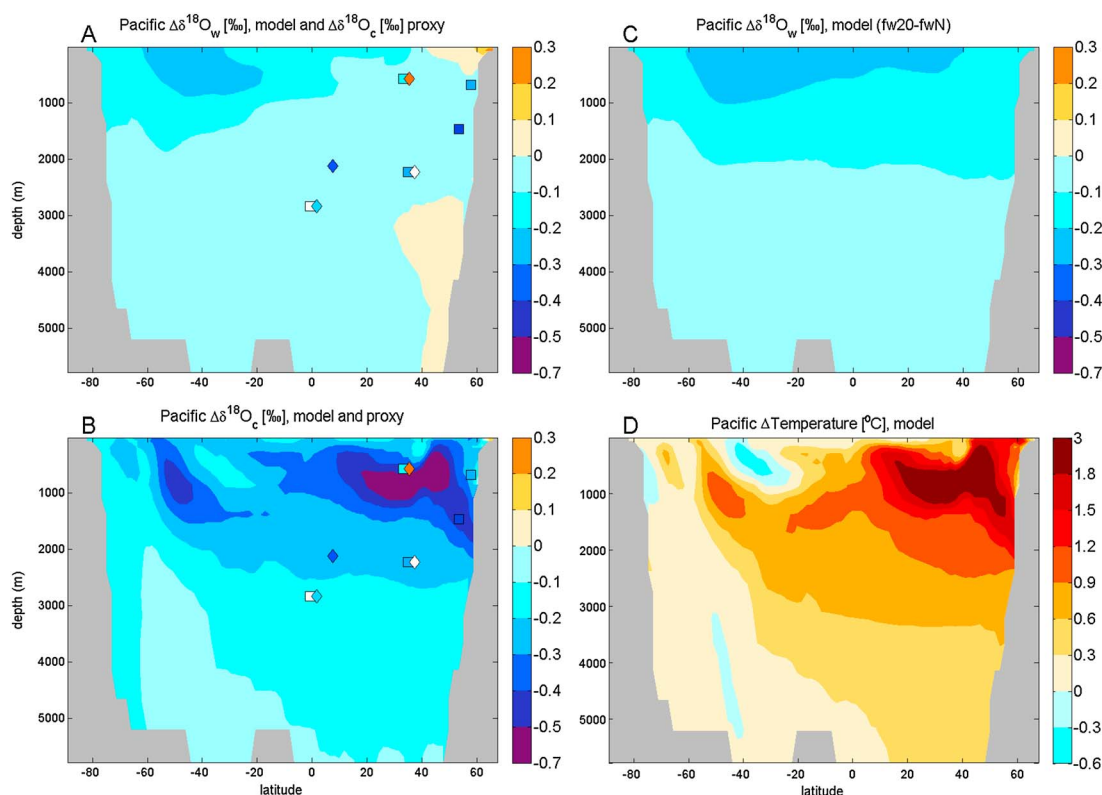


Figure 5. Anomalies (Δ , year 2000 minus year 0) simulated in experiment fw20 in the Pacific Ocean (zonal average), superimposed by paleoproxy $\delta^{18}O_c$ anomalies for HS1 (squares) and HS4 (diamonds): (a) $\delta^{18}O_w$; (b) $\delta^{18}O_c$; (c) meltwater signal; and (d) temperature.

paleoproxy records for HS1 (Figure 4c). The largest discrepancy is found in core MD95-2010 where the model underestimates the decrease by $\sim 1\text{‰}$.

3.3. Comparison of Simulated Changes in $\delta^{18}O$ and SST With Paleoproxy Records in the Pacific Ocean

NADW cessation leads to a $\sim 0.2\text{‰}$ $\delta^{18}O_w$ increase at the surface of the North Pacific (Figure 3a). Enhanced NPDW formation increases the northward heat transport in the North Pacific and the transport of low latitude ^{18}O -rich seawater, resulting in positive SST anomalies of up to 3°C in the North Pacific. Such seesaw connection between the North Atlantic and the North Pacific has been found previously [Saenko et al., 2004; Okazaki et al., 2010; Menviel et al., 2011; Huiskamp and Meissner, 2012].

In the Pacific Ocean, the simulated $\delta^{18}O_w$ anomaly exceeds -0.2‰ in the South Pacific above 1000 m depth (Figure 5a). In the deep North Pacific the simulated anomalies are generally smaller than 0.1‰ and can be assumed to be too low to be detectable in data. In our simulation, the temperature effect is the dominant reason for $\delta^{18}O_c$ anomalies in the North Pacific. For example, the 2°C temperature increase centered at 600 m depth in the North Pacific (Figure 5d) leads to a $\delta^{18}O_c$ decrease of 0.6‰ (Figure 5b). This warming was identified in a dye tracer propagation analysis (not shown here) as caused by a reduction in AABW and the formation of relatively warm NPDW. North Pacific cores record anomalies ranging between -0.45‰ (JPC51) and 0.3‰ (ODP893A). As six out of nine HS records show negative $\delta^{18}O_c$ anomalies deviating by less than 0.3‰ from simulated $\delta^{18}O_c$, the model appears to be in relatively good agreement with the data (Figure 5b). It should be noted that the temporal bounds of the Heinrich Stadials are particularly difficult to establish for proxy records in the North Pacific due to the weakness of the signal and the probable time lags [Friedrich and Timmermann, 2012]. In the Pacific HS4 and HS1 are thus set at fixed dates (38.8–40.2 ka B.P. for HS4 and 15.5–17.5 ka B.P. for HS1).

3.4. Deconvolution of the Contributing Factors to $\delta^{18}O$ Anomalies

$\delta^{18}O_w$ anomalies can be separated into a “meltwater” and a “circulation and climate” effect. The meltwater effect describes the addition of ^{18}O -depleted meltwater to the North Atlantic and its subsequent propagation. This part of the signal can be estimated in simulations with non-isotope-enabled models

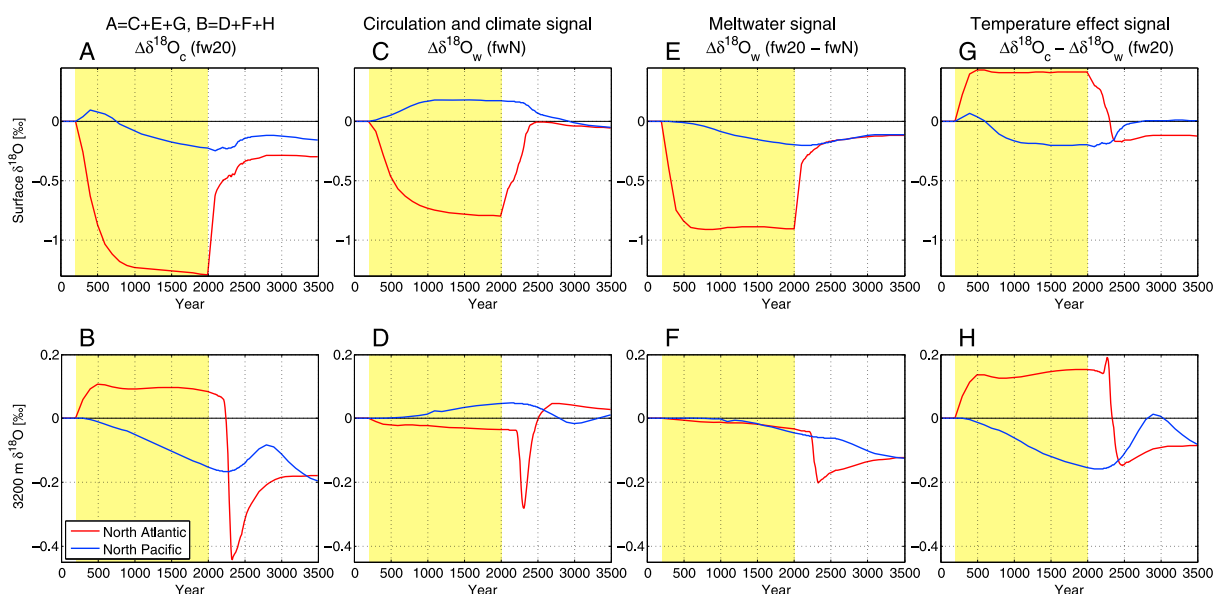


Figure 6. Average $\delta^{18}\text{O}$ anomalies in the North Atlantic (red line) and the North Pacific (blue line) between 30°N and 60°N (top row) at the surface and (bottom row) at 3200 m depth. (a and b) The $\delta^{18}\text{O}_c$ anomalies for experiment fw20; (c and d) $\delta^{18}\text{O}_w$ anomalies for experiment fwN; (e and f) difference between $\Delta\delta^{18}\text{O}_w$ (fw20) and $\Delta\delta^{18}\text{O}_w$ (fwN), representing the meltwater signal; and (g and h) difference between $\Delta\delta^{18}\text{O}_c$ (fw20) and $\Delta\delta^{18}\text{O}_w$ (fw20), representing the temperature effect. Yellow area represents the time span of the freshwater flux.

[Friedrich and Timmermann, 2012; Gebbie, 2012]. The circulation and climate effect describes the impact of changes in precipitation and evaporation on $\delta^{18}\text{O}_w$ and also variations in $\delta^{18}\text{O}_w$ due to changes in ocean circulation. In addition, the circulation and climate effect also includes changes in sea ice formation and melt as well as river discharge; however, these have only a minor effect in our simulations. The circulation and climate effect can only be represented in isotope-enabled models. Finally, changes in $\delta^{18}\text{O}_c$ will depend on changes in $\delta^{18}\text{O}_w$ plus changes in water temperature, as the isotopic fractionation during foraminiferal calcification is temperature dependent (temperature effect signal).

In simulation fwN, the meltwater added into the North Atlantic does not include an isotopic signature and thus the meltwater does not directly impact $\delta^{18}\text{O}_w$. Therefore, fwN tracks the circulation and climate signal. We can then estimate the meltwater signal by differentiating between $\delta^{18}\text{O}_w$ anomalies of experiments fw20 and fwN. As seen in Figure 3c, the addition of low $\delta^{18}\text{O}$ water into the North Atlantic leads to a negative $\delta^{18}\text{O}_w$ anomaly at the surface of the North Atlantic of up to -1.6‰ . This anomaly decreases southward and with depth (Figure 4d). By comparing Figures 3a and 3c, we can also see that the changes in surface currents, precipitation, and evaporation are responsible for about half of the negative $\delta^{18}\text{O}_w$ anomalies at the surface of the Atlantic and for the small positive $\delta^{18}\text{O}_w$ anomaly at the surface of the North Pacific. The $\delta^{18}\text{O}_w$ anomaly due to meltwater input is about -0.2‰ at the surface of the South Atlantic and South Pacific (Figure 5c). The magnitude of $\delta^{18}\text{O}_w$ change is sensitive to the isotopic content of meltwater (see supporting information).

Figures 6a and 6b show time series of $\delta^{18}\text{O}_c$ anomalies for the fw20 simulation, averaged over the North Atlantic (in red) and the North Pacific Ocean (in blue), at the surface (top row) and at 3200 m depth (bottom row). In Figures 6c–6h the $\delta^{18}\text{O}_c$ signal is decomposed into its three contributing factors: the “circulation and climate change signal” (Figures 6c and 6d, $\Delta\delta^{18}\text{O}_w$ in fwN), the meltwater signal (Figures 6e and 6f, difference between fw20 $\Delta\delta^{18}\text{O}_w$ and fwN $\Delta\delta^{18}\text{O}_w$), and temperature effect signal (6g and 6h, difference between $\Delta\delta^{18}\text{O}_c$ and $\Delta\delta^{18}\text{O}_w$ in fw20).

At the surface of the North Atlantic (Figure 6, top row, red lines), negative $\delta^{18}\text{O}_w$ anomalies are due to weaker advection of low latitude, high $\delta^{18}\text{O}_w$ waters (Figure 6c). Furthermore, lower SSTs reduce evaporation, which leads to an additional decrease in $\delta^{18}\text{O}_w$. The addition of depleted meltwater contributes an additional 0.9‰ $\delta^{18}\text{O}_w$ decrease in the North Atlantic (Figure 6e). However, lower SSTs induce a 0.4‰ increase in $\delta^{18}\text{O}_c$ (Figure 6g).

At the surface of the North Pacific (Figure 6, top row, blue lines), increased NPDW formation (see section 3.1 and Figure 2) enhances the advection of warm, ^{18}O -rich low latitude waters to the North Pacific. In addition,

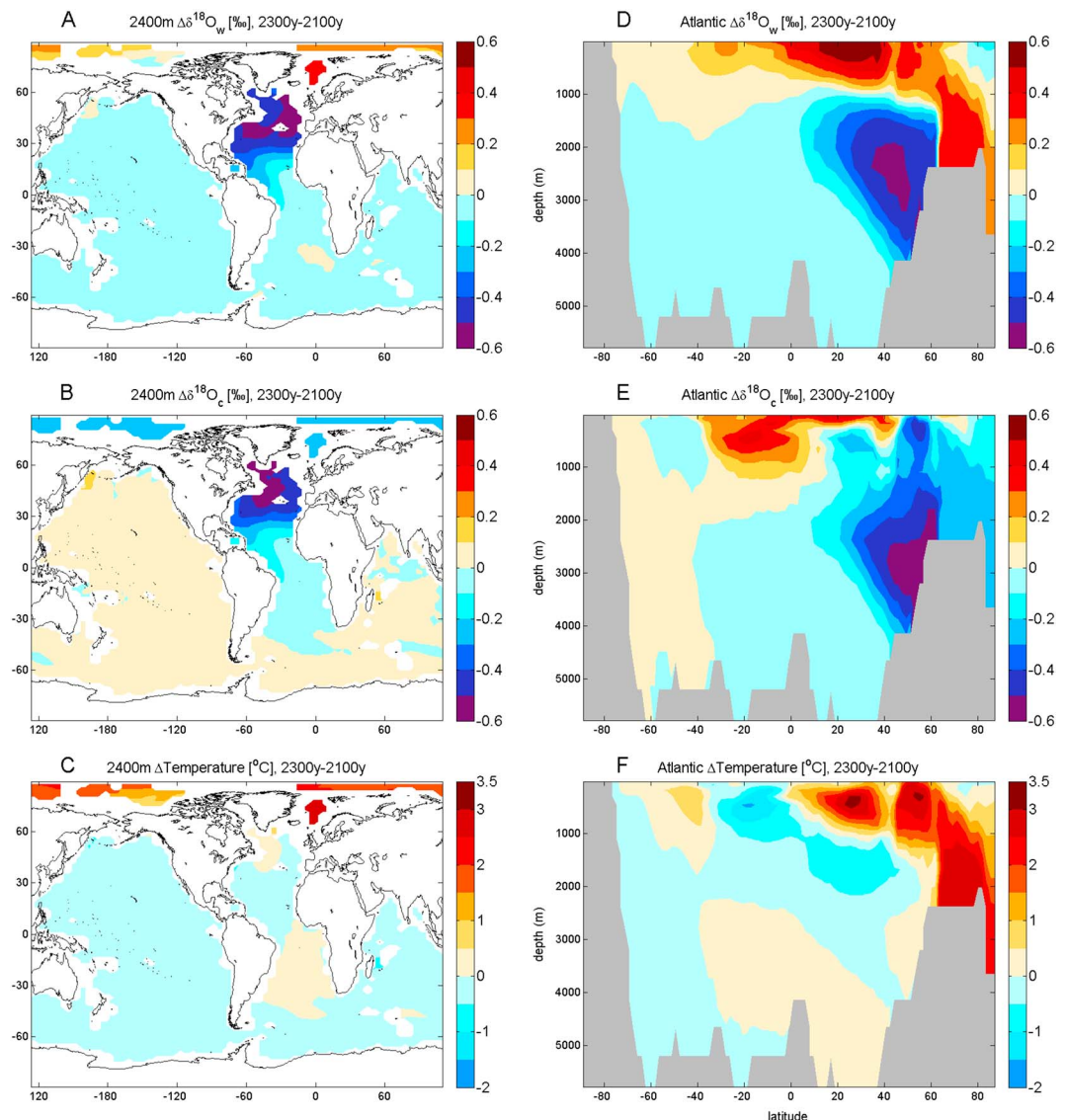


Figure 7. Anomalies simulated in experiment fw20 during the AMOC recovery (year 2300 minus year 2100) (a–c) at 2400 m depth and (d–f) in the Atlantic Ocean (zonal average). Figures 7a and 7d show $\delta^{18}O_w$ anomalies; Figures 7b and 7e show $\delta^{18}O_c$ anomalies; and Figures 7c and 7f show temperature anomalies.

higher SSTs in the North Pacific lead to an increase in evaporation, which enhances the $\delta^{18}O_w$ increase (Figure 6c). On the other hand, higher SSTs induce a 0.2‰ decrease in $\delta^{18}O_c$ (Figure 6g).

An AMOC resumption and NPDW cessation, which both take place during years 2000–2400 (Figure 2), revert the circulation and climate signal in the surface ocean (Figure 6c). At the end of the simulations, North Atlantic and North Pacific meltwater $\delta^{18}O_w$ anomalies converge near the equilibrium value expected for the amount of meltwater released (–0.12‰ for fw20, Figures 6e and 6f).

At depth in the North Pacific (Figure 6, bottom row, blue lines), the NPDW formation induces a warming (Figure 5d), which leads to a continuous $\delta^{18}O_c$ decrease until model year 2200 (Figure 6h).

During the AMOC resumption, deep North Atlantic $\delta^{18}O_c$ rapidly decreases by 0.5‰ and subsequently partly recovers by 0.25‰ within the next 500 years (Figure 6b, red line). Hence, the maximum anomaly in the deep North Atlantic lags the maximum anomaly in the surface North Atlantic by about 400 years—the time it takes for the AMOC to recover. The AMOC resumption leads to the advection of low $\delta^{18}O_w$ water to the deep North Atlantic (Figures 6d, 6f, and 7d). The resulting decrease in $\delta^{18}O_c$ reaches a maximum of about –0.6‰ below 2000 m depth (Figure 7b and 7e). This signal, seen as a $\delta^{18}O_c$ spike in Figure 6b, resembles anomalies found

in several North Atlantic cores, e.g., MD95-2010 [Dokken and Jansen, 1999], ENAM93-21 [Rasmussen et al., 1996], and SO82-5 [Krevelde et al., 2000]. These anomalies have been attributed to ^{18}O -depleted surface water masses, which were entrained to the deep ocean by dense brines, rejected during sea ice formation, while the large-scale overturning motion was weakened or shut off. The associated mechanism became known as the sea ice brine hypothesis and places sea ice formation as a main facilitator of local deep convection during glacial stadials [Dokken and Jansen, 1999]. However, the spike seen in our simulations is not caused by sea ice formation. It is due to a rapid and large-scale resumption of NADW formation, transiently bringing anomalously low $\delta^{18}\text{O}_w$ surface waters to deeper depths (Figures 7a and 7d). This AMOC resumption is also associated with a warming of the deep North Atlantic, due to a replacement of cold AABW with warmer NADW. This warming enhances the deep Atlantic negative $\delta^{18}\text{O}_c$ spike (Figure 6h). However, the maximum warming of the deep North Atlantic occurs about 200 years after the maximum $\delta^{18}\text{O}_w$ decrease seen in the circulation and climate signal (Figures 6d and 6h). Hence, in our simulation the two signals do not reinforce each other in forming the $\delta^{18}\text{O}_c$ spike (Figure 6b) but affect different parts of the ocean at different times. Regardless, the decrease in $\delta^{18}\text{O}_w$ is large enough (up to -0.6‰) to still cause a negative spike in $\delta^{18}\text{O}_c$ if the freshly formed NADW replaces a warmer water mass, as simulated in our LOVECLIM simulation.

It should be noted that the UVic ESCM has two stable states under LGM boundary conditions: one state with a weak AMOC and the other with a shutdown AMOC. To switch between these states, external buoyancy forcing is applied to the North Atlantic. For example, the triggered recovery of AMOC in this study might have been more vigorous and faster (or slower) than the real recovery of the AMOC at the end of HS1 and HS4. Contrary to MD95-2010 [Dokken and Jansen, 1999] and ENAM93-21 [Rasmussen et al., 1996] proxy records, the simulated depleted benthic $\delta^{18}\text{O}_c$ signal lags the planktic $\delta^{18}\text{O}_c$ signal by approximately 400 years. This apparent discrepancy could be due to the relatively slow recovery of the AMOC in our simulations.

Finally, a comparison of the time series in Figures 6c–6h reveals that in both the surface North Atlantic and the surface North Pacific, the three factors for Heinrich Stadial induced $\delta^{18}\text{O}_c$ changes of a similar magnitude, while the deep ocean $\delta^{18}\text{O}_c$ changes are driven mostly by changes in temperature (Figure 6h). At model year 2000, all three contributing factors to surface $\delta^{18}\text{O}_c$ anomalies are larger in the North Atlantic than in the North Pacific, while at 3200 m depth they are of similar magnitude in both basins.

4. Discussion and Conclusions

Despite representing a highly idealized scenario, the simulated surface $\delta^{18}\text{O}$ anomalies agree in parts reasonably well with the paleoproxy records (Figures 3a and 3b). Addition and advection of low $\delta^{18}\text{O}_w$ meltwater leads to significant negative $\delta^{18}\text{O}_w$ anomalies in the entire North Atlantic. In addition, changes in surface currents, precipitation, and evaporation induced by the weakened AMOC reinforce these negative $\delta^{18}\text{O}_w$ anomalies in the North Atlantic surface waters. The associated North Atlantic cooling only partially offsets this anomaly; therefore, negative $\delta^{18}\text{O}_c$ anomalies are also simulated over the whole North Atlantic in agreement with most proxy records (Figure 3). However, this is in contrast with two paleoproxy records from the Iberian margin (MD95-2040 and MD99-2339), which display positive $\delta^{18}\text{O}_c$ anomalies during HS4 (Figure 3b, diamonds).

It should be noted that fresh water was added over a broad region of the North Atlantic in our model simulations and that we are using a coarse-resolution ocean model, which cannot resolve eddies or narrow coastal currents. Therefore, our simulations cannot account for the exact origin and pathway of the low $\delta^{18}\text{O}$ water in the North Atlantic [Condrón and Winsor, 2012; Spence et al., 2013]. In addition, the meltwater forcing used here was probably too large, as the freshwater equivalent of 22 m sea level rise leads to an overestimation of the $\delta^{18}\text{O}_c$ decrease. Based on our results and the results of Roche et al. [2014], an equivalent 10 m sea level rise with an isotopic signature of -20‰ would likely lead to a better model-proxy agreement for HS1 and HS4. In the Pacific Ocean, paleoproxy records and modeling results suggest negative $\delta^{18}\text{O}_c$ anomalies, except for marine sediment core MD02-2529, which displays a strong $\delta^{18}\text{O}_c$ increase. This increase has been interpreted as a salinification of the Eastern Equatorial Pacific due to reduced moisture transport from the Atlantic to the Pacific [Richter and Xie, 2010].

A different approach would be necessary to estimate a more accurate time- and location-dependent meltwater scenario with varying $\delta^{18}\text{O}$ ratios. For example, a fully coupled and oxygen-isotope-enabled ice sheet, ocean, sea ice, atmosphere model could provide a better estimate of the isotopic content of meltwater and its variability over the duration of the Heinrich event. Furthermore, it might provide more accurate magnitudes

of the freshwater fluxes associated with Heinrich events. Although *Siddall et al.* [2003] estimated a sea level rise of ~20 m during HS4, other studies provide lower estimates; for example, *Chappell* [2002] suggests a sea level rise of about 9 m. Finally, the proxy reconstructions are also likely to reflect processes that are not accounted for by the model. For example, planktic foraminifera may move vertically in the water column throughout their life cycle [*Duplessy et al.*, 1981; *Bradley*, 1999], thus flattening out the Heinrich $\delta^{18}\text{O}_c$ signal. It should also be noted that core data may be affected by dating errors and insufficient sampling frequency.

The fact that the simulated subsurface $\delta^{18}\text{O}_c$ increase in the Atlantic is in better agreement with HS4 records than with HS1 records (Figure 4b) raises the possibility that temperature anomalies in the North Atlantic were different between HS1 and HS4, with strong subsurface Atlantic cooling only occurring during HS4. Our results therefore indicate that the North Atlantic deep and intermediate circulation might have been different during the two events. They suggest a partial replacement of Glacial North Atlantic Intermediate Water with colder Southern Hemisphere sourced water masses during HS4, while the residence time of North Atlantic intermediate and deep waters might have increased during HS1 leading to a warming due to heat diffusion [*Marcott et al.*, 2011; *Flückiger et al.*, 2006; *Mignot et al.*, 2007]. The difference between the two events could also simply be due to the deglacial warming of deep and intermediate Atlantic waters during HS1.

Similar to *Friedrich and Timmermann* [2012], our study finds a significant lag between the surface and deep ocean meltwater signals (Figures 6e and 6f) due to an AMOC shutdown. The meltwater signal does not spread throughout the deep ocean with NADW; instead, as in *Rahmstorf* [2002], it spreads near the surface into the Southern Ocean, from where it is exported into the deep ocean with AABW, eventually reaching both the deep North Atlantic and the deep North Pacific at approximately the same pace (Figure 6f, roughly year 1000 to year 2200). However, since the meltwater signal in the deep ocean is relatively weak, such lag between the surface and the deep ocean is not seen in $\Delta\delta^{18}\text{O}_c$ (Figures 6a and 6b), where the signal is dominated by the temperature effect signal and the circulation and climate signal. Caution should therefore be taken when analyzing isotope anomalies simulated as simple passive tracers in non-isotope-enabled models.

Overall, the three contributing factors to changes in surface $\delta^{18}\text{O}_c$ (temperature effect, circulation and climate effect, and meltwater effect) are of similar magnitude, while changes in benthic $\delta^{18}\text{O}_c$ are mainly dictated by the temperature effect (Figure 6). In the surface ocean, the largest changes are seen in the Atlantic basin, while in the deep ocean, changes in $\delta^{18}\text{O}_c$ are of similar magnitude in the Atlantic and Pacific Oceans. Our results are in agreement with an earlier study by *Gebbie* [2012], who found, using an inverse method based on a tracer transport model of modern-day ocean circulation, that changes in glacial-deglacial $\delta^{18}\text{O}_c$ at an Iberian margin core were contributed nearly equally by $\delta^{18}\text{O}_w$ and temperature. However, unlike the results presented here, *Gebbie* [2012] finds the $\delta^{18}\text{O}_w$ influence on $\delta^{18}\text{O}_c$ to be twice as large as temperature in the eastern Pacific.

Finally, this is to our knowledge the first modeling study that simulates the ~0.5‰ $\delta^{18}\text{O}_c$ depletion in the deep North Atlantic found in sediment records during Heinrich Stadials [e.g., *Rasmussen et al.*, 1996; *Dokken and Jansen*, 1999; *Krevelde et al.*, 2000; *Rasmussen and Thomsen*, 2004; *Hillaire-Marcel and de Vernal*, 2008; *Meland et al.*, 2008]. Our results (Figures 6b and 7) do not support the hypothesis that such decrease was caused by sea ice variability and the resulting brine water formation, a mechanism that has been brought forward in the past [*Vidal et al.*, 1998; *Dokken and Jansen*, 1999] but which also has been questioned recently [*Bauch and Bauch*, 2001; *Stanford et al.*, 2011; *Brennan et al.*, 2013]. Instead, we show that such anomalies could occur as a consequence of a rapid resumption of the AMOC at the end of a large meltwater or Heinrich event.

Acknowledgments

We thank four anonymous reviewers and the Editor, Christopher Charles, for providing constructive suggestions on earlier versions of this manuscript. We also thank Paul Valdes for his valuable comments. This study was funded by the Australian Research Council (FT10010043, DE150100107) and supported by an award under the Merit Allocation Scheme on the NCI National Facility at the Australian National University. W. Bagniewski is grateful for a UNSW Tuition Fee Scholarship. The modeling data described in this paper can be obtained by contacting the corresponding author.

References

- Ahn, J., and E. J. Brook (2014), Siple Dome ice reveals two modes of millennial CO_2 change during the last ice age, *Nat. Commun.*, 5, 3723, doi:10.1038/ncomms4723.
- Alley, R. B., T. K. Dupont, B. R. Parizek, S. Anandakrishnan, D. E. Lawson, G. J. Larson, and E. B. Evenson (2006), Outburst flooding and the initiation of ice-stream surges in response to climatic cooling: A hypothesis, *Geomorphology*, 75(1), 76–89.
- Archer, D. (1996), A data-driven model of the global calcite lysocline, *Global Biogeochem. Cycles*, 10(3), 511–526.
- Baertschi, P. (1976), Absolute ^{18}O content of standard mean ocean water, *Earth Planet. Sci. Lett.*, 31(3), 341–344.
- Bauch, D., and H. A. Bauch (2001), Last glacial benthic foraminiferal $\delta^{18}\text{O}$ anomalies in the polar North Atlantic: A modern analogue evaluation, *J. Geophys. Res.*, 106(C5), 9135–9143.
- Berger, A. L. (1978), Long-term variations of caloric insolation resulting from the Earth's orbital elements, *Quat. Res.*, 9(2), 139–167.
- Bradley, R. S. (1999), *Paleoclimatology: Reconstructing Climates of the Quaternary*, Academic, San Diego, Calif.
- Brady, E. C., and B. L. Otto-Bliessner (2011), The role of meltwater-induced subsurface ocean warming in regulating the Atlantic meridional overturning in glacial climate simulations, *Clim. Dyn.*, 37(7–8), 1517–1532.
- Brennan, C. E., A. J. Weaver, M. Eby, and K. J. Meissner (2012), Modelling oxygen isotopes in the University of Victoria Earth System Climate Model for pre-industrial and Last Glacial Maximum conditions, *Atmos. Ocean*, 50(4), 447–465.

- Brennan, C. E., K. J. Meissner, M. Eby, C. Hillaire-Marcel, and A. J. Weaver (2013), Impact of sea ice variability on the oxygen isotope content of seawater under glacial and interglacial conditions, *Paleoceanography*, *28*(3), 388–400, doi:10.1002/palo.20036.
- Caissie, B. E., J. Brigham-Grette, K. T. Lawrence, T. D. Herbert, and M. S. Cook (2010), Last Glacial Maximum to Holocene sea surface conditions at Umnak Plateau, Bering Sea, as inferred from diatom, alkenone, and stable isotope records, *Paleoceanography*, *25*, PA1206, doi:10.1029/2008PA001671.
- Carlson, A. E., D. W. Oppo, R. E. Came, A. N. LeGrande, L. D. Keigwin, and W. B. Curry (2008), Subtropical Atlantic salinity variability and Atlantic meridional circulation during the last deglaciation, *Geology*, *36*(12), 991–994.
- Chappell, J. (2002), Sea level changes forced ice breakouts in the Last Glacial cycle: New results from coral terraces, *Quat. Sci. Rev.*, *21*(10), 1229–1240.
- Charles, C. D., J. Lynch-Stieglitz, U. S. Ninnemann, and R. G. Fairbanks (1996), Climate connections between the hemisphere revealed by deep sea sediment core/ice core correlations, *Earth Planet. Sci. Lett.*, *142*(1), 19–27.
- Condron, A., and P. Winsor (2012), Meltwater routing and the Younger Dryas, *Proc. Natl. Acad. Sci.*, *109*(49), 19,928–19,933.
- Craig, H. (1957), Isotopic standards for carbon and oxygen and correction factors for mass-spectrometric analysis of carbon dioxide, *Geochim. Cosmochim. Acta*, *12*(1), 133–149.
- Davies, M. H., A. C. Mix, J. S. Stoner, J. A. Addison, J. Jaeger, B. Finney, and J. Wiest (2011), The deglacial transition on the southeastern Alaska Margin: Meltwater input, sea level rise, marine productivity, and sedimentary anoxia, *Paleoceanography*, *26*, PA2223, doi:10.1029/2010PA002051.
- Deplazes, G., et al. (2013), Links between tropical rainfall and North Atlantic climate during the last glacial period, *Nat. Geosci.*, *6*(3), 213–217.
- Dokken, T. M., and E. Jansen (1999), Rapid changes in the mechanism of ocean convection during the last glacial period, *Nature*, *401*(6752), 458–461.
- Duplessy, J. C., P. L. Blanc, and A. W. Be (1981), Oxygen-18 enrichment of planktonic foraminifera due to gametogenic calcification below the euphotic zone, *Science*, *213*(4513), 1247–1250.
- Eby, M., K. Zickfeld, A. Montenegro, D. Archer, K. J. Meissner, and A. J. Weaver (2009), Lifetime of anthropogenic climate change: Millennial time scales of potential CO₂ and surface temperature perturbations, *J. Clim.*, *22*(10), 2501–2511.
- Fleitmann, D., et al. (2009), Timing and climatic impact of Greenland interstadials recorded in stalagmites from northern Turkey, *Geophys. Res. Lett.*, *36*, L19707, doi:10.1029/2009GL040050.
- Flückiger, J., R. Knutti, and J. W. White (2006), Oceanic processes as potential trigger and amplifying mechanisms for Heinrich events, *Paleoceanography*, *21*, PA2014, doi:10.1029/2005PA001204.
- Friedrich, T., and A. Timmermann (2012), Millennial-scale glacial meltwater pulses and their effect on the spatiotemporal benthic δ¹⁸O variability, *Paleoceanography*, *27*, PA3215, doi:10.1029/2012PA002330.
- Gebbie, G. (2012), Tracer transport timescales and the observed Atlantic-Pacific lag in the timing of the Last Termination, *Paleoceanography*, *27*, PA3225, doi:10.1029/2011PA002273.
- Gherardi, J.-M., L. Labeyrie, S. Nave, R. Francois, J. F. McManus, and E. Cortijo (2009), Glacial-interglacial circulation changes inferred from ²³¹Pa/²³⁰Th sedimentary record in the North Atlantic region, *Paleoceanography*, *24*, PA2204, doi:10.1029/2008PA001696.
- González, C., and L. M. Dupont (2010), Tropical vegetation evidence for rapid sea level changes associated with Heinrich Events, *IOP Conf. Ser. Earth Environ. Sci.*, *9*(1), 12,003, doi:10.1088/1755-1315/9/1/012003.
- Heinrich, H. (1988), Origin and consequences of cyclic ice rafting in the northeast Atlantic Ocean during the past 130,000 years, *Quat. Res.*, *29*(2), 142–152.
- Hendy, I. L., J. P. Kennett, E. B. Roark, and B. L. Ingram (2002), Apparent synchronicity of submillennial scale climate events between Greenland and Santa Barbara Basin, California from 30–10 ka, *Quat. Sci. Rev.*, *21*(10), 1167–1184.
- Hibler, W. D., III (1979), A dynamic thermodynamic sea ice model, *J. Phys. Oceanogr.*, *9*(4), 815–846.
- Hill, T. M., J. P. Kennett, D. K. Pak, R. J. Behl, C. Robert, and L. Beaufort (2006), Pre-Bölling warming in Santa Barbara Basin, California: Surface and intermediate water records of early deglacial warmth, *Quat. Sci. Rev.*, *25*(21), 2835–2845.
- Hillaire-Marcel, C., and A. de Vernal (2008), Stable isotope clue to episodic sea ice formation in the glacial North Atlantic, *Earth Planet. Sci. Lett.*, *268*(1), 143–150.
- Hillaire-Marcel, C., J.-F. Hélie, J. McKay, and A. de Vernal (2008), Elusive isotopic properties of deglacial meltwater spikes into the North Atlantic: Example of the final drainage of Lake Agassiz, *Can. J. Earth Sci.*, *45*(11), 1235–1242.
- Hodell, D. A., K. A. Venz, C. D. Charles, and U. S. Ninnemann (2003), Pleistocene vertical carbon isotope and carbonate gradients in the South Atlantic sector of the Southern Ocean, *Geochem. Geophys. Geosyst.*, *4*, 1004, doi:10.1029/2002GC000367.
- Hodell, D. A., H. F. Evans, J. E. Channell, and J. H. Curtis (2010), Phase relationships of North Atlantic ice-rafted debris and surface-deep climate proxies during the last glacial period, *Quat. Sci. Rev.*, *29*(27), 3875–3886.
- Huber, C., M. Leuenberger, R. Spahni, J. Flückiger, J. Schwander, T. F. Stocker, S. Johnsen, A. Landais, and J. Jouzel (2006), Isotope calibrated Greenland temperature record over Marine Isotope Stage 3 and its relation to CH₄, *Earth Planet. Sci. Lett.*, *243*(3), 504–519.
- Huiskamp, W. N., and K. J. Meissner (2012), Oceanic carbon and water masses during the Mystery Interval: A model-data comparison study, *Paleoceanography*, *27*, PA4206, doi:10.1029/2012PA002368.
- Hunke, E. C., and J. K. Dukowicz (1997), An elastic-viscous-plastic model for sea ice dynamics, *J. Phys. Oceanogr.*, *27*(9), 1849–1867.
- Kalnay, E., et al. (1996), The NCEP/NCAR 40-year Reanalysis project, *Bull. Am. Meteorol. Soc.*, *77*(3), 437–471.
- Kissel, C., C. Laj, A. M. Piotrowski, S. L. Goldstein, and S. R. Hemming (2008), Millennial-scale propagation of Atlantic deep waters to the glacial Southern Ocean, *Paleoceanography*, *23*, PA2102, doi:10.1029/2008PA001624.
- Kreveland, S. v., M. Sarnthein, H. Erlenkeuser, P. Grootes, S. Jung, M. J. Nadeau, U. Pflaumann, and A. Voelker (2000), Potential links between surging ice sheets, circulation changes, and the Dansgaard-Oeschger Cycles in the Irminger Sea, 60–18 kyr, *Paleoceanography*, *15*(4), 425–442.
- Labeyrie, L., C. Waelbroeck, E. Cortijo, E. Michel, and J. C. Duplessy (2005), Changes in deep water hydrology during the last deglaciation, *C. R. Geosci.*, *337*(10–11), 919–927.
- Lea, D. W., D. K. Pak, C. L. Belanger, H. J. Spero, M. A. Hall, and N. J. Shackleton (2006), Paleoclimate history of Galapagos surface waters over the last 135,000 yr, *Quat. Sci. Rev.*, *25*(11), 1152–1167.
- Leduc, G., L. Vidal, K. Tachikawa, F. Rostek, C. Sonzogni, L. Beaufort, and E. Bard (2007), Moisture transport across Central America as a positive feedback on abrupt climatic changes, *Nature*, *445*(7130), 908–911.
- Lewis, S. C., A. N. LeGrande, M. Kelley, and G. A. Schmidt (2010), Water vapour source impacts on oxygen isotope variability in tropical precipitation during Heinrich events, *Clim. Past*, *6*(3), 325–343.

- Little, M. G., R. R. Schneider, D. Kroon, B. Price, T. Bickert, and G. Wefer (1997), Rapid palaeoceanographic changes in the Benguela Upwelling System for the last 160,000 years as indicated by abundances of planktonic foraminifera, *Palaeoogeogr. Palaeoclimatol. Palaeoecol.*, *130*(1), 135–161.
- Liu, Z., et al. (2009), Transient simulation of last deglaciation with a new mechanism for Bølling-Allerød warming, *Science*, *325*(5938), 310–314.
- Lynch-Stieglitz, J., M. W. Schmidt, and W. B. Curry (2011), Evidence from the Florida Straits for Younger Dryas ocean circulation changes, *Paleoceanography*, *26*, PA1205, doi:10.1029/2010PA002032.
- Lynch-Stieglitz, J., M. W. Schmidt, L. G. Henry, W. B. Curry, L. C. Skinner, S. Mulitza, R. Zhang, and P. Chang (2014), Muted change in Atlantic overturning circulation over some glacial-aged Heinrich events, *Nat. Geosci.*, *7*(2), 144–150.
- MacAyeal, D. R. (1993), Binge/purge oscillations of the Laurentide ice sheet as a cause of the North Atlantic's Heinrich events, *Paleoceanography*, *8*(6), 775–784.
- Marchitto, T. M., W. B. Curry, J. Lynch-Stieglitz, S. P. Bryan, K. M. Cobb, and D. C. Lund (2014), Improved oxygen isotope temperature calibrations for cosmopolitan benthic foraminifera, *Geochim. Cosmochim. Acta*, *130*, 1–11, doi:10.1016/j.gca.2013.12.034.
- Marcott, S. A., et al. (2011), Ice-shelf collapse from subsurface warming as a trigger for Heinrich events, *Proc. Natl. Acad. Sci.*, *108*(33), 13,415–13,419.
- Martrat, B., J. O. Grimalt, N. J. Shackleton, L. de Abreu, M. A. Hutterli, and T. F. Stocker (2007), Four climate cycles of recurring deep and surface water destabilizations on the Iberian margin, *Science*, *317*(5837), 502–507.
- McManus, J. F., R. Francois, J. M. Gherardi, L. D. Keigwin, and S. Brown-Leger (2004), Collapse and rapid resumption of Atlantic meridional circulation linked to deglacial climate changes, *Nature*, *428*(6985), 834–837.
- Meissner, K. J., A. Schmittner, E. C. Wiebe, and A. J. Weaver (2002), Simulations of Heinrich events in a coupled ocean-atmosphere-sea ice model, *Geophys. Res. Lett.*, *29*(14), 1671, doi:10.1029/2001GL013514.
- Meissner, K. J., A. J. Weaver, H. D. Matthews, and P. M. Cox (2003), The role of land surface dynamics in glacial inception: A study with the UVic Earth System Model, *Clim. Dyn.*, *21*(7–8), 515–537.
- Meissner, K. J., B. I. McNeil, M. Eby, and E. C. Wiebe (2012), The importance of the terrestrial weathering feedback for multimillennial coral reef habitat recovery, *Global Biogeochem. Cycles*, *26*, GB3017, doi:10.1029/2011GB004098.
- Meland, M. Y., T. M. Dokken, E. Jansen, and K. Hevrøy (2008), Water mass properties and exchange between the Nordic seas and the northern North Atlantic during the period 23–6 ka: Benthic oxygen isotopic evidence, *Paleoceanography*, *23*, PA1210, doi:10.1029/2007PA001416.
- Menviel, L., A. Timmermann, O. E. Timm, and A. Mouchet (2011), Deconstructing the Last Glacial termination: The role of millennial and orbital-scale forcings, *Quat. Sci. Rev.*, *30*(9–10), 1155–1172.
- Menviel, L., M. H. England, K. J. Meissner, A. Mouchet, and J. Yu (2014a), Atlantic-Pacific seesaw and its role in outgassing CO₂ during Heinrich events, *Paleoceanography*, *29*, 58–70, doi:10.1002/2013PA002542.
- Menviel, L., A. Timmermann, T. Friedrich, and M. H. England (2014b), Hindcasting the continuum of Dansgaard-Oeschger variability: Mechanisms, patterns and timing, *Clim. Past*, *10*(1), 63–77.
- Mignot, J., A. Ganopolski, and A. Levermann (2007), Atlantic subsurface temperatures: Response to a shutdown of the overturning circulation and consequences for its recovery, *J. Clim.*, *20*(19), 4884–4898.
- Millo, C., M. Sarnthein, A. Voelker, and H. Erlenkeuser (2006), Variability of the Denmark Strait overflow during the last glacial maximum, *Boreas*, *35*(1), 50–60.
- Oba, T., T. Irino, M. Yamamoto, M. Murayama, A. Takamura, and K. Aoki (2006), Paleooceanographic change off central Japan since the last 144,000 years based on high-resolution oxygen and carbon isotope records, *Global Planet. Change*, *53*(1), 5–20.
- Okazaki, Y., A. Timmermann, L. Menviel, N. Harada, A. Abe-Ouchi, M. O. Chikamoto, A. Mouchet, and H. Asahi (2010), Deepwater formation in the North Pacific during the last glacial termination, *Science*, *329*(5988), 200–204.
- O'Neil, J. R. (1968), Hydrogen and oxygen isotope fractionation between ice and water, *J. Phys. Chem.*, *72*(10), 3683–3684.
- Pacanowski, R. C. (1995), MOM 2, documentation, user's guide and reference manual, GFDL, Princeton, N. J.
- Pahnke, K., R. Zahn, H. Elderfield, and M. Schulz (2003), 340,000-year centennial-scale marine record of Southern Hemisphere climatic oscillation, *Science*, *301*(5635), 948–952.
- Peck, V. L., I. R. Hall, R. Zahn, F. Grousset, S. R. Hemming, and J. D. Scourse (2007), The relationship of Heinrich events and their European precursors over the past 60 ka BP: A multi-proxy ice-rafted debris provenance study in the North East Atlantic, *Quat. Sci. Rev.*, *26*(7), 862–875.
- Peltier, W. R. (1994), Ice age paleotopography, *Science*, *265*(5169), 195–201.
- Praetorius, S. K., and A. C. Mix (2014), Synchronization of North Pacific and Greenland climates preceded abrupt deglacial warming, *Science*, *345*(6195), 444–448.
- Rahmstorf, S. (2002), Ocean circulation and climate during the past 120,000 years, *Nature*, *419*(6903), 207–214.
- Rasmussen, T. L., and E. Thomsen (2004), The role of the North Atlantic Drift in the millennial timescale glacial climate fluctuations, *Palaeoogeogr. Palaeoclimatol. Palaeoecol.*, *210*(1), 101–116.
- Rasmussen, T. L., and E. Thomsen (2009), Stable isotope signals from brines in the Barents Sea: Implications for brine formation during the last glaciation, *Geology*, *37*(10), 903–906.
- Rasmussen, T. L., E. Thomsen, L. Labeyrie, and T. C. van Weering (1996), Circulation changes in the Faeroe-Shetland Channel correlating with cold events during the last glacial period (58–10 ka), *Geology*, *24*(10), 937–940.
- Richter, I., and S.-P. Xie (2010), Moisture transport from the Atlantic to the Pacific basin and its response to North Atlantic cooling and global warming, *Clim. Dyn.*, *35*(2–3), 551–566.
- Roche, D. M., D. Paillard, T. Caley, and C. Waelbroeck (2014), LGM hosing approach to Heinrich Event 1: Results and perspectives from data-model integration using water isotopes, *Quat. Sci. Rev.*, *106*, 247–261.
- Rohling, E. J., R. Marsh, N. C. Wells, M. Siddall, and N. R. Edwards (2004), Similar meltwater contributions to glacial sea level changes from Antarctic and northern ice sheets, *Nature*, *430*(7003), 1016–1021.
- Rosenthal, Y., D. W. Oppo, and B. K. Linsley (2003), The amplitude and phasing of climate change during the last deglaciation in the Sulu Sea, western equatorial Pacific, *Geophys. Res. Lett.*, *30*(8), 1428, doi:10.1029/2002GL016612.
- Rühlemann, C., S. Mulitza, G. Lohmann, A. Paul, M. Prange, and G. Wefer (2004), Intermediate depth warming in the tropical Atlantic related to weakened thermohaline circulation: Combining paleoclimatic data and modeling results for the last deglaciation, *Paleoceanography*, *19*, PA1025, doi:10.1029/2003PA000948.
- Saenko, O. A., A. Schmittner, and A. J. Weaver (2004), The Atlantic-Pacific seesaw, *J. Clim.*, *17*(11), 2033–2038.
- Saikku, R., L. Stott, and R. Thunell (2009), A bi-polar signal recorded in the western tropical Pacific: Northern and Southern Hemisphere climate records from the Pacific warm pool during the last Ice Age, *Quat. Sci. Rev.*, *28*(23), 2374–2385.

- Sarnthein, M., et al. (2001), Fundamental modes and abrupt changes in North Atlantic circulation and climate over the last 60 ky—concepts, reconstruction and numerical modeling, in *The Northern North Atlantic: A Changing Environment*, pp. 365–410, Springer, Berlin.
- Schmidt, M. W., and J. Lynch-Stieglitz (2011), Florida Straits deglacial temperature and salinity change: Implications for tropical hydrologic cycle variability during the Younger Dryas, *Paleoceanography*, *26*, PA4205, doi:10.1029/2011PA002157.
- Schmidt, M. W., H. J. Spero, and D. W. Lea (2004), Links between salinity variation in the Caribbean and North Atlantic thermohaline circulation, *Nature*, *428*(6979), 160–163.
- Schmittner, A., A. Oschlies, H. D. Matthews, and E. D. Galbraith (2008), Future changes in climate, ocean circulation, ecosystems, and biogeochemical cycling simulated for a business-as-usual CO₂ emission scenario until year 4000 AD, *Global Biogeochem. Cycles*, *22*, GB1013, doi:10.1029/2007GB002953.
- Semtner, A. J. (1976), A model for the thermodynamic growth of sea ice in numerical investigations of climate, *J. Phys. Oceanogr.*, *6*(3), 379–389.
- Shackleton, N. J. (1967), Oxygen isotope analyses and Pleistocene temperatures re-assessed, *Nature*, *215*(5096), 15–17.
- Shackleton, N. J. (1974), Attainment of isotopic equilibrium between ocean water and the benthonic foraminifera genus *Uvigerina*: Isotopic changes in the ocean during the last glacial, *Colloques Internationaux du C.N.R.S.*, *219*, 203–210.
- Shackleton, N. J., M. A. Hall, and E. Vincent (2000), Phase relationships between millennial-scale events 64,000–24,000 years ago, *Paleoceanography*, *15*(6), 565–569.
- Siddall, M., E. J. Rohling, A. Almogi-Labin, C. Hemleben, D. Meischner, I. Schmelzer, and D. Smeed (2003), Sea-level fluctuations during the last glacial cycle, *Nature*, *423*(6942), 853–858.
- Siddall, M., E. J. Rohling, W. G. Thompson, and C. Waelbroeck (2008), Marine isotope stage 3 sea level fluctuations: Data synthesis and new outlook, *Reviews of Geophysics*, *46*, RG4003, doi:10.1029/2007RG000226.
- Skinner, L. C., N. J. Shackleton, and H. Elderfield (2003), Millennial-scale variability of deep-water temperature and $\delta^{18}\text{O}_{dw}$ indicating deep-water source variations in the Northeast Atlantic, 0–34 cal. ka BP, *Geochem. Geophys. Geosyst.*, *4*(12), 1098, doi:10.1029/2003GC000585.
- Spence, P., O. A. Saenko, W. Sijp, and M. H. England (2013), North Atlantic climate response to Lake Agassiz drainage at coarse and ocean eddy-permitting resolutions, *J. Clim.*, *26*(8), 2651–2667.
- Stanford, J. D., E. J. Rohling, S. Bacon, A. P. Roberts, F. E. Grousset, and M. Bolshaw (2011), A new concept for the paleoceanographic evolution of Heinrich event 1 in the North Atlantic, *Quat. Sci. Rev.*, *30*(9), 1047–1066.
- Thornalley, D. J. R., S. Barker, W. S. Broecker, H. Elderfield, and I. N. McCave (2011), The deglacial evolution of North Atlantic deep convection, *Science*, *331*(6014), 202–205.
- Urey, H. C. (1948), Oxygen isotopes in nature and in the laboratory, *Science*, *108*(2810), 489–496.
- Veum, T., E. Jansen, M. Arnold, I. Beyer, and J.-C. Duplessy (1992), Water mass exchange between the North Atlantic and the Norwegian Sea during the past 28,000 years, *Nature*, *356*(6372), 783–785.
- Vidal, L., L. Labeyrie, E. Cortijo, M. Arnold, J. C. Duplessy, E. Michel, S. Becque, and T. C. E. Van Weering (1997), Evidence for changes in the North Atlantic Deep Water linked to meltwater surges during the Heinrich events, *Earth Planet. Sci. Lett.*, *146*(1), 13–27.
- Vidal, L., L. Labeyrie, and T. C. E. v Weering (1998), Benthic $\delta^{18}\text{O}$ records in the North Atlantic over the last glacial period (60–10 kyr): Evidence for brine formation, *Paleoceanography*, *13*(3), 245–251, doi:10.1029/98PA00315.
- Voelker, A. H. L., and L. de Abreu (2011), A review of abrupt climate change events in the northeastern Atlantic Ocean (Iberian Margin): Latitudinal, longitudinal, and vertical gradients, in *Abrupt Climate Change: Mechanisms, Patterns, and Impacts*, edited by H. Rashid, L. Polyak, and E. Mosley-Thompson, pp. 15–37, AGU, Washington, D. C.
- Voelker, A. H. L., S. M. Lebreiro, J. Schönfeld, I. Cacho, H. Erlenkeuser, and F. Abrantes (2006), Mediterranean outflow strengthening during Northern Hemisphere coolings: A salt source for the glacial Atlantic?, *Earth Planet. Sci. Lett.*, *245*(1), 39–55.
- Waelbroeck, C., C. Levi, J. C. Duplessy, L. Labeyrie, E. Michel, E. Cortijo, F. Bassinot, and F. Guichard (2006), Distant origin of circulation changes in the Indian Ocean during the last deglaciation, *Earth Planet. Sci. Lett.*, *243*(1–2), 244–251.
- Waelbroeck, C., L. C. Skinner, L. Labeyrie, J. C. Duplessy, E. Michel, N. Vazquez Riveiros, J. M. Gherardi, and F. Dewilde (2011), The timing of deglacial circulation changes in the Atlantic, *Paleoceanography*, *26*, PA3213, doi:10.1029/2010PA002007.
- Wang, Y. J., H. Cheng, R. L. Edwards, Z. S. An, J. Y. Wu, C. C. Shen, and J. A. Dorale (2001), A high-resolution absolute-dated late Pleistocene monsoon record from Hulu Cave, China, *Science*, *294*(5550), 2345–2348.
- Weaver, A. J., et al. (2001), The UVic Earth System Climate Model: Model description, climatology, and applications to past, present and future climates, *Atmos. Ocean*, *39*(4), 361–428.
- Weinelt, M., M. Sarnthein, U. Pflaumann, H. Schulz, S. Jung, and H. Erlenkeuser (1996), Ice-free Nordic seas during the last glacial maximum? Potential sites of deep-water formation, *Paleoclimates*, *1*(4), 283–309.
- Weinelt, M., E. Vogelsang, M. Kucera, U. Pflaumann, M. Sarnthein, A. Voelker, H. Erlenkeuser, and B. A. Malmgren (2003), Variability of North Atlantic heat transfer during MIS 2, *Paleoceanography*, *18*(3), 1071, doi:10.1029/2002PA000772.
- Weldeab, S., R. R. Schneider, M. Kölling, and G. Wefer (2005), Holocene African droughts relate to eastern equatorial Atlantic cooling, *Geology*, *33*(12), 981–984.
- Weldeab, S., R. R. Schneider, and M. Kölling (2006), Deglacial sea surface temperature and salinity increase in the western tropical Atlantic in synchrony with high latitude climate instabilities, *Earth Planet. Sci. Lett.*, *241*(3), 699–706.
- Weldeab, S., D. W. Lea, R. R. Schneider, and N. Andersen (2007), 155,000 years of West African monsoon and ocean thermal evolution, *Science*, *316*(5829), 1303–1307.
- Ziegler, M., D. Nürnberg, C. Karas, R. Tiedemann, and L. J. Lourens (2008), Persistent summer expansion of the Atlantic Warm Pool during glacial abrupt cold events, *Nat. Geosci.*, *1*(9), 601–605.